FEBS Letters 587 (2013) 1405–1410

journal homepage: www.FEBSLetters.org

Quality control system response to stochastic growth of amyloid fibrils

Simone Pigolotti [a,*], Ludvig Lizana [b,c], Daniel Otzen [d], Kim Sneppen [b]

[a] Dept. de Fisica i Eng. Nuclear, Universitat Politecnica de Catalunya Edif. GAIA, Rambla Sant Nebridi s/n, 08222 Terrassa, Barcelona, Spain
[b] Niels Bohr Institute, Blegdamsvej 17, DK-2100 Copenhagen, Denmark
[c] Integrative Science Lab, Department of Physics, Umeå University, SE-901 87 Umeå, Sweden
[d] University of Aarhus, iNANO, Department of Molecular Biology and Genetics Center for Insoluble Protein Structures (inSPIN), Gustav Wieds Vej 10 Aarhus C, Denmark

ARTICLE INFO

Article history:
Received 17 December 2012
Revised 28 February 2013
Accepted 6 March 2013
Available online 21 March 2013

Edited by Michael R. Bubb

Keywords:
Protein aggregation
Neurodegenerative disease
Stochastic dynamics
Spiky oscillation
Proteasome–lysosome

ABSTRACT

We introduce a stochastic model describing aggregation of misfolded proteins and degradation by the protein quality control system in a single cell. Aggregate growth is contrasted by the cell quality control system, that attacks them at different stages of the growth process, with an efficiency that decreases with their size. Model parameters are estimated from experimental data. Two qualitatively different behaviors emerge: a homeostatic state, where the quality control system is stable and aggregates of large sizes are not formed, and an oscillatory state, where the quality control system periodically breaks down, allowing for formation of large aggregates. We discuss how these periodic breakdowns may constitute a mechanism for the development of neurodegenerative diseases.

1. Introduction

Protein aggregation and formation of amyloid fibrils are a subject of intense experimental and theoretical study. A main motivation is that such phenomena, and in particular the formation of cytotoxic pre-amyloid species and larger inclusion bodies, is a common theme underlying most known neurodegenerative diseases [1–7]. Besides structural studies, several attempts have been made to build up coarse-grained models, describing the kinetic of the aggregation process in vitro. One of their key features is the existence of a nucleation mechanism [8]. During later stages of the aggregation, the possibility of aggregates to fragment also becomes important [9,10]. Recent works reported that, in some cases, in vitro filament growth is not gradual but occurs in almost discrete steps [11,12]. Several other models have been proposed, including more detailed mechanisms [13,14].

While in vitro amyloid aggregation is quite well characterized, much less is known about the corresponding dynamics in vivo. This is the main focus in this paper. Beside the limitations of single-cell and culture experiments compared to the in vitro case, there are also a number of theoretical challenges. For example, aggregates typically grow in vitro on timescales of hours or days. In contrast, it is unclear why aggregates grow in vivo in a time frame of week to years, as shown by long-term imaging of amyloid accmulation in murine brains [15].

A large number of studies demonstrates that the ubiquitin–proteasome system (UPS) is implicated in neurodegenerative disorders [16,17]. It has been suggested that insoluble inclusion bodies form due to an impaired UPS function, given that proteasomal inhibitors lead to inclusion bodies and neuronal apoptosis [18–20]. Proteasomal activity is reduced in Parkinsons Disease (PD), characterized by intracellular amyloid deposits of the protein α-synuclein (αSN) [21]. Pathogenic αSN mutants (found in familial versions of PD) can as oligomers and fibrils bind to proteasome and inhibit it directly [22], while overproduction of mutant αSN makes cells sensitive to proteasome inhibitors [23]. Further, aggregated proteins per se impair proteasomal functioning [24–26]. Another degradation pathway involves macroautophagy, an intracellular catabolic system in which cytoplasmic components are delivered into lysosomes for degradation. Indeed, neurodegenerative diseases appear to be most closely linked to macroautophagy. Parkin, a protein that is mutated in autosomal recessive forms of PD, appears to act as a signal for selective autophagy of dysfunctional mitochondria in PD [27], while the pathogenic αSN mutants A53T and A30P also bind a receptor for chaperone-mediated autophagy, inhibiting this pathway [28]. There is a relation to UPS in that protein aggregates can be degraded by selective autophagy via ubiquitin tagging [29,30], while impairment of

* Corresponding author. Fax: +34 93 739 8000.
E-mail address: simone.pigolotti@upc.edu (S. Pigolotti).

0014-5793/$36.00
http://dx.doi.org/10.1016/j.febslet.2013.03.018

autophagy system in neurons leads to neurodegeneration and ubiquitin-positive inclusions [31,32]. Furthermore, A53T αSN overproduction inhibits both proteasomal and lysosomal activity [33].

In a previous study, we explored in a simple two-stage model the consequences of the interaction between α-SN and the UPS system [34]. We found a transition between a state in which the UPS system effectively prevents aggregation, and one in which spiky oscillations are observed. During such spikes, the UPS is impaired, allowing for growth of aggregates. However, a more mechanicistic description of the aggregation kinetics in vivo is still lacking, making parameter estimation from experimental data problematic. Furthermore, we did not include the possibility of lysosomal degradation.

To address these issues, we propose a mechanicistic model describing the battle between protein aggregation and the quality control system (QCS) in a single cell. The aggregation process is implemented stochastically. Aggregates are formed when a nucleation threshold is passed, and grow according to the existing concentration of monomers, as in [13]. Further, large aggregates can break into smaller fragments. We study the interaction of this dynamics with the response of the protein QCS. Its action is modeled as an enzymatic degradation, whose efficiency depends on the size of the aggregate. In the first part of the manuscript, we identify this system with the UPS, as it is better characterized from a biochemical point of view. As larger fragments are more likely to be attacked by autophagy, in the second part we generalize of the model to describe lysosomal degradation. Most of the parameters in the our model have been measured experimentally. For some of them, it is difficult to find quantitative estimates, due to current limitations in the ability to monitor cellular aggregation with a precision approaching that of in vitro studies. However, we anticipate that the rapid development in imaging and e.g. fluorescence labeling techniques will close this gap in the foreseeable future [15,35–37].

2. Model

We define f_n as the number of free aggregates made up of n monomers present in a cell, so that f_1 is the number of free monomers, or aggregation-prone proteins. We model the action of the QCS as an enzymatic degradation: the agent produced by the cell degrading the filaments, denoted by E, can bind to a filament of size n (f_n) to form a complex C_n, which is then degraded. While the enzymatic reaction scheme is standard for protein degradation such as that operated by the proteasome, it should be considered more speculative for a large body such as a lysosome. However, it captures the basic essence of a degradation operating after some processing time also in this case. We therefore adopt the same scheme in the two cases, but modify the corresponding parameters to take into account the different size and efficiency of the two agents. The interplay between f_n,E and C_n is summarized in the reactions (R1)–(R7) of Fig. 1 and discussed below.

In analogy with existing literature [9,13], we describe the dynamics of aggregate formation in terms of two basic processes: (R1) growth by attachment of monomers to the fibril ends, and (R2) random breakage of aggregates into smaller fragments. Reactions (R1) and (R2) occur at rates γ and β, respectively. We also introduce a simple nucleation mechanism: the rate at which two monomers bind (R1′) $f_1 + f_1 \xrightarrow{\gamma'} f_2$ is much smaller than (R1), i.e. $\gamma' \ll \gamma$, corresponding to a barrier for dimer formation. The dynamics encoded in (R1), (R1′) and (R2) has shown to be consistent with results of in vitro aggregation experiments [13]. In addition, we consider a constant production of monomers at rate μ (R3).

Molecules of the degradation enzyme E are produced at rate α (R4) and degraded at rate δ per molecule (R5). Degradation of aggregates is assumed to take place as a two-step process. First, E can bind to a fibril of a given size n to form a complex C_n (R6). We assume that monomers are not attacked by the QCS. Then, in a time proportional to n, the aggregate is entirely degraded, while the enzyme is released (R7). The choice of a degradation time being proportional to n is a simplification, due to the level of biochemical characterization of the degrading agents. A more general assumption would be to introduce functions $\eta(n)$ and $\nu(n)$, different for different agents, describing the spectrum of aggregates that each of them can effectively bind and degrade. Finally, notice that E represents the number of units of the *free* degradation enzyme, not counting those bound to aggregates.

3. Choice of model parameters

In this section, we discuss the estimates of the rates. All rates are expressed per molecule per day (per cell). For binary reactions, it is relevant to estimate the cell volume. The average diameter of a dopaminergic neuron is from 10 to 20 μm (see e.g. [41]). This corresponds to an approximate cell volume of $v \approx 10^{-11} l$.

Studies on insulin [39] report fibril growth rates around 0.3 monomers per fibril per second at a monomer concentration of 0.17 mM. Similar studies on other molecules [40] report similar values. Given the cell volume above, one single monomer in a cell corresponds to a concentration of $1/(N_A v) \approx 2 \times 10^{-13} M$ where N_A is the Avogadro number. The growth rate per fibril per monomer is then $0.25 \times 10^{-9}\,s^{-1}$, i.e. approximately 2×10^{-5} monomers per fibril per day. Ref. [39] estimates from reaction rate arguments that one every 10^5 encounter events between filaments and monomer results in attachment. Estimates of nucleation barriers lead to an activation rate being 8–9 orders of magnitudes smaller than the

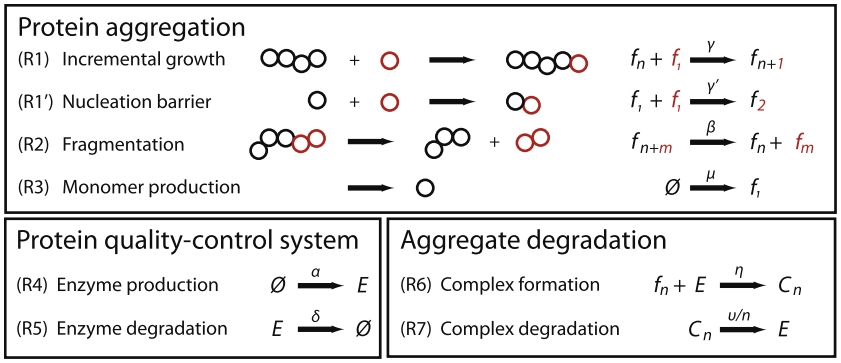

Fig. 1. Scheme of the reactions: protein aggregation (top panel) and degradation by the quality control system (bottom right panel). The dynamics of the QCS is shown in the bottom left panel. The "enzyme" represents either the proteasome or the lysosome, depending on the parameters choice.

growth rate γ [13]. This rate could however be different in vivo, since cell condition can significantly favor/disfavor the formation of nucleation seeds. We choose a relatively high nucleation rate, $\gamma' = 2 \times 10^{-10}$ per day per molecule pair per cell volume. We fix a filament breakage rate $\beta = 10^{-3}$ [13]. The production rate of monomers α is left as a free parameter. Since its value is typically large, to speed up the simulations we implemented an alternative reaction in which 100 monomers at a time are produced with a rate $\alpha/100$. We checked in shorter simulations that such approximation does not alter significantly the results, thanks to the typical high numbers of monomers.

We move now to the parameters related to the proteasome. Proteasome lifetime is estimated to be 8–15 days in the cell [42,43], leading to a degradation rate $\delta = 0.1$. The proteasome production rate α is left as a free parameter. On general grounds, we may expect the proteasome to bind better to the filaments than to a monomer, leading to a complex formation η being larger than γ. We choose $\eta = 0.02$, corresponding to one successful binding event every 100 encounters. A lower value of η would make the proteasome less effective and simply result in a higher threshold value for α to observe oscillations, without affecting the qualitative features of the model. As the degradation rate of individual molecules by the proteasome is on the order of minutes, we choose $\nu = 10^3$. Parameters corresponding to the lysosome case are discussed in the results section.

4. Results

Our model of Fig. 1 describe reactions taking place in a single cell. As numbers of molecules can be small, stochastic number fluctuations must be taken into account. Therefore, we implemented the reactions via the Gillespie algorithm [38], where at each time reactions are chosen proportionally to its probability. We start our analysis by identifying the enzyme with the UPS, which we refer to simply as the proteasome. Although there is little quantitative information on the rates of breakdown of different aggregates by proteasomes, this system has been studied in great detail and is an undisputed central player in cellular degradation pathways. Fig. 2, right shows the dynamics of the model with the parameter choice from Section 3. After a short transient, the system reaches an homeostatic state, where there is a chemical balance between proteasome concentration and the formation of aggregates. In the figure, filaments and complexes (bound filaments) represent a sum over all sizes excluding the monomers f_1, that is $\sum_{n>} f_n$ and $\sum_{n>1} C_n$. The figure shows that their concentrations fluctuate moderately around well defined average values which means that the proteasome is fully functioning and keeps the total aggregate concentration down.

In this regime, aggregates of large size are unlikely to be formed. Fig. 2 shows that the distribution of filament sizes is also stationary. In Appendix A, we study the stochiometric rate equations corresponding to our model, assuming that the fragmentation rate β can be neglected compared to the degradation by the QCS. The steady state solution shows that filament sizes are exponentially distributed in this approximation. A comparison between this steady-state solution and the outcome of the Gillespie simulation of the stochastic model is presented in the inset of Fig. 2, right panel. The theoretical curve, without any free parameter, predicts very closely the outcome of the simulation. The hypothesis that the fragmentation rate is essentially irrelevant in this regime is therefore confirmed. This is a radical difference compared with in vitro results, where fibrils grow at a much higher speed, up to a size which is limited by the fragmentation rate and, in experiments, by the available pool of aggregating peptide chains [13].

If the monomer production rate μ is increased, homeostasis breaks down and oscillations emerge (Fig. 3, left panel). Despite the fact that simulations are stochastic, the period of the oscillations is remarkably regular. This is a consequence of the (average) high copy number of all proteins involved. In this regime, there are dramatic drops in proteasome concentration which stays low for long periods of time, leading to a buildup of larger and larger fibrillar aggregates. The QCS cannot cope in this case with the amount of aggregates present in the system, resulting in a slower decay of the aggregate size distribution. Eventually, bound proteasome is suddenly released after degradation of the aggregates, and a proteasome concentration close to the homeostatic level is recovered. This means that the system alternates between states in which the QCS is functioning, and short periods in which the proteasome is impaired. During such periods, aggregates of large size can be produced, as shown in the right panel of Fig. 3. This is a consequence of the fact that the growth dynamics, in the absence of degradation, is faster than the recovery time of the QCS. In particular, the largest formed aggregate is of a size about 10^3 monomers, as opposed to 10^2 in the stable homeostatic case of Fig. 2. This maximum size clearly depends on the modeling choice of a linear dependence of the degradation time on the aggregate size: assuming a sharper dependence would make the QCS practically unable to degrade large aggregates, providing a mechanism for Lewy

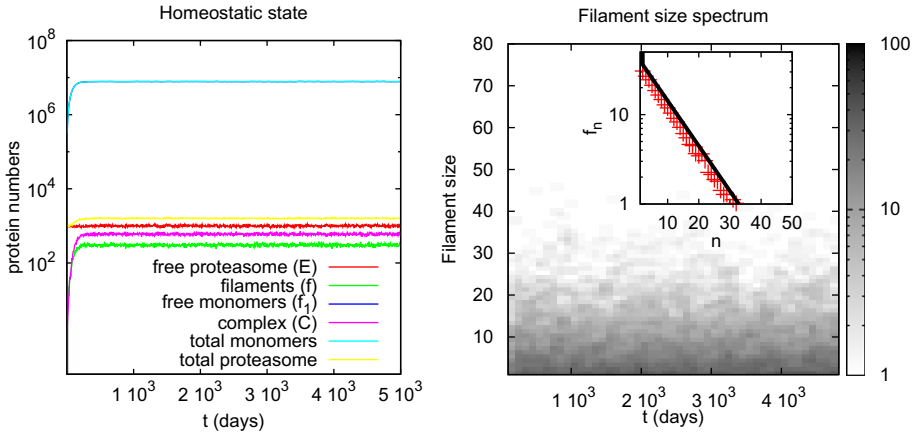

Fig. 2. Homeostatic state. (left) Number of molecules (or aggregates) as a function of time. Dark and blue curves are almost coincident, as the vast majority of monomers are not aggregated with this parameter choice, (right) Size distribution of free filaments. The gray scale shows the number of aggregates that has a given size n at a time t. Parameters are: $\gamma = 2 \times 10^{-5}$, $\gamma' = 2 \times 10^{-10}$, $\beta = 10^{-3}$, $\mu = 6 \times 10^4$, $\alpha = 10^2$, $\delta = 0.1$, $\eta = 0.02$, $\nu = 10^2$. Inset shows the average free filament size distribution, compared with the prediction of Eq. (5).

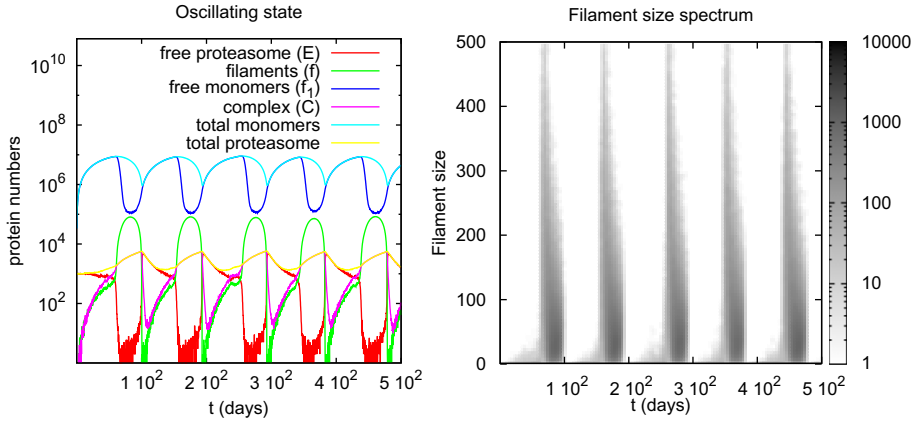

Fig. 3. Oscillatory state. Parameters are same as Fig. 2 but μ is three times larger, $\mu = 1.8 \times 10^5$. (left) number of molecules (or aggregates) as a function of time. (right) Size distribution of free filaments.

bodies formation. Notice also how, in the stable regime, aggregate monomers constitute a small fraction of the total monomer pool. This can be seen by comparing the almost overlapping dark and light blue curves in Fig. 2. Conversely, in Fig. 3, one observe a large fraction of monomers being aggregated during the periods when the proteasome is impaired.

We conclude by remarking that, starting from the homeostatic state of Fig. 2, oscillations can be triggered by varying also other parameters; in particular, reducing the proteasome production rate α, and/or the proteasome degradation efficiency ν. On the other hand, simulations (not shown) suggest that this triggering does not depend much on the fragmentation rate, as filaments are mostly actively degraded by the QCS.

4.1. Lysosomal degradation

Lysosomal degradation is less characterized biochemically compared to proteasomal degradation. The lack of detailed experimental information about lysosomal turnover in the cell requires us to explore a range of parameter values which we consider biologically plausible. As previously discussed, we represent the lysosome as an efficient enzyme present in small numbers. We assumed a production rate $\alpha = 1$ lysosome per day, and a degradation rate of $\delta = 0.1$ lysosomes per day which corresponds to an average of 10 lysosomes per cell at steady state. We assumed furthermore that the rate at which the enzyme degrades aggregates (per aggregate size) is $\nu = 2 \times 10^3$, i.e. 20 times more efficient than the proteasome.

Fig. 4 shows the results of a simulation for this parameter choice. Even in this case we observe an oscillatory destabilization of the homeostatic state, as the higher efficiency of lysosomes are compensated by the lower numbers. The main difference with Fig. 3 is that the period of the oscillations is much more irregular. This is a consequence of the enzyme being present in small numbers, making stochastic fluctuations more important. We verified that we robustly obtained similar dynamical behaviors by varying the parameters. The only observed differences when increasing the efficiency (or the number) of lysosomes are that the crisis of the QCS are less frequent and the typical recovery time faster. Conversely, decreasing further the lysosome efficiency drives the system into a state in which the cell cannot cope most of the time with the amount of growing filaments. Finally, we remark that, while the same transition observed here is present in the deterministic version of the model such as that of the rate equations presented in the appendix, [1], noise is crucial as it enlarges the region of parameter space where oscillations should be expected. Indeed, by simulating rate equations corresponding to the parameter choices of Figs. 2 and 3, we found that they still are in the stable homeostatic state.

5. Discussion

In this paper we studied the interplay between sequential growth of amyloid fibrils and its degradation by the QCS in a single cell. The main result is that, in the regime in which the QCS cannot cope with the amount of fibrils, destabilisation of the

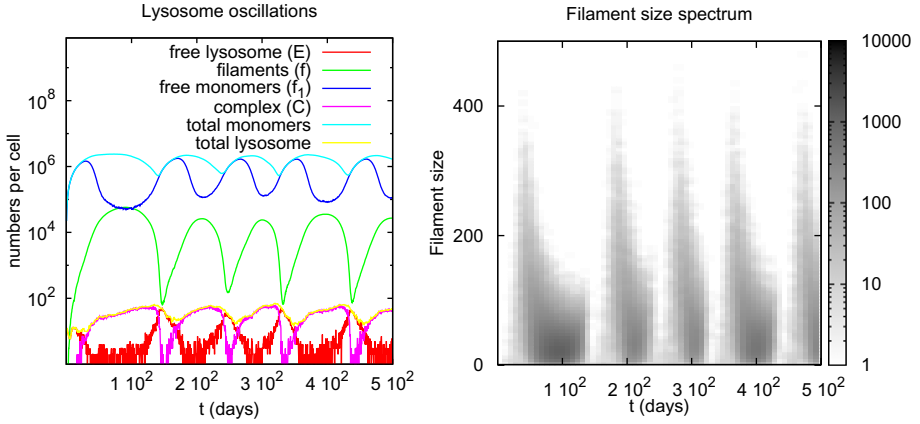

Fig. 4. Oscillations in the presence of lysosome. Parameters are as in Fig. 2, except $\alpha = 1$ and $\nu = 2 \times 10^3$. As usual, (left) number of molecules (or aggregates, or lysosomes) as a function of time, (right) size distribution of filaments. The period of oscillations is more stochastic as the degrading agent is present in small numbers in this case.

homeostatic state gives rise to an oscillatory regime. While such transition was already observed in the simple model presented in [34], our new results demonstrate how oscillations can occur for values of parameters being compatible, to the best of our knowledge, with physiological conditions. The resulting oscillations are characterized by time lapses in which the QCS is functioning and prevents aggregation, separated by time windows in which the QCS is impaired and fibrils of large sizes can grow. The period of such oscillations depends on the parameter choice but is typically on the scale of months. This behavior strongly contrast with the dynamics in the absence of the QCS [13], which is much faster and where oscillations do not appear. The model thus predicts that the net growth of aggregates is a slow process, reminiscent to the remarkably slow development of neurodegenerative diseases [15]. Finally, we have shown that when the agent degrading the aggregates is present in large numbers, the resulting oscillations tend to be very regular and almost deterministic, while when the numbers are smaller oscillations are more irregular.

There are clearly a number of generalisations one can consider to account for more accurate experimental evidences, such as the possibility of different interconnected repair systems, that attack aggregates at different stages of the growth process and with different efficiencies depending on the aggregate size. Our model should be considered as a minimal mechanistic model displaying such non-trivial phenomenology.

Acknowledgements

This work was funded by the Danish National Research Foundation through the Center for Models of Life (CMOL). L.L acknowledges the financial support by the Knut and Alice Wallenberg Foundation. D.E.O. is funded by the Danish Research Foundation (inSPIN) and the Lundbeck Foundation (BioNET 2). We thank P.H. Jensen for discussions.

Appendix A. Steady state solution of the rate equations

In this Appendix, we present the stochiometric rate equations corresponding to the reactions in Fig. 1 and calculate their steady-state solution. We simplify the calculation by neglecting the fragmentation rate, $\beta = 0$. In this approximation, the rate equations can be simply written as

$$\begin{aligned}
&\frac{d}{dt}f_1 = \mu - \gamma f_1\left(\sum_{n>1} f_n\right) - \gamma' f_1^2\\
&\frac{d}{dt}f_2 = \gamma' f_1^2 - \gamma f_1 f_2 - \eta E f_2\\
&\frac{d}{dt}f_n = \gamma f_1 (f_{n-1} - f_n) - \eta E f_n \quad \text{for } n > 2\\
&\frac{d}{dt}C_n = \eta f_n E - \frac{v}{n} C_n\\
&\frac{d}{dt}E = \alpha - \delta E - \sum_{n>1}\left(\eta E f_n - \frac{v}{n} C_n\right)
\end{aligned} \tag{1}$$

where we assumed that, for all proteins involved, the numbers per cell are large enough to be considered as continuous variables. From the last two equations, we readily obtain that at steady state $E = \alpha/\delta$ and $C_n = n\alpha f_n/(\delta v)$. To obtain an expression for the fibril distribution f_n, we define $\sigma = \sum_{n>1} f_n$. Writing the equation for σ (i.e. summing the equations for f_n for $2 \leqslant n < \infty$) and imposing steady state yields

$$\gamma' f_1^2 - \frac{\eta\alpha}{\delta}\sigma = 0 \rightarrow \sigma = \frac{\delta\gamma'}{\eta\alpha} f_1^2. \tag{2}$$

Substituting into the equation for f_1 leads to

$$\frac{\delta\gamma\gamma'}{\eta\alpha} f_1^3 + \gamma' f_1^2 - \mu = 0. \tag{3}$$

One can show by standard methods that the above third order equation admits a unique positive real solution. Let us call this positive solution $\bar{f}$. Substituting $\bar{f}$ into the equations for f_2 and for the f_n, $n > 2$ leads to an exponential distribution

$$f_n = A\ \exp(-Bn) \quad \text{for } n > 1 \tag{4}$$

characterized by the parameters

$$\begin{aligned}
A &= \frac{\gamma'\left(\gamma\bar{f} + \eta\frac{\alpha}{\delta}\right)}{\gamma^2}\\
B &= \ln\left(\frac{\gamma\bar{f} + \frac{\eta\alpha}{\delta}}{\gamma\bar{f}}\right).
\end{aligned} \tag{5}$$

References

[1] Ross, C.A. and Poitier, M.A. (2004) Protein aggregation and neurodegenerative disease. Nat. Med. 10, S10–S17.
[2] Chiti, F. and Dobson, C.M. (2006) Protein misfolding, functional amyloid, and human disease. Annu. Rev. Biochem. 75, 333–366.
[3] Uversky, V.N. (2010) Mysterious oligomerization of the amyloidogenic proteins. FEBS J. 277 (14), 2940–2953.
[4] Adams, D., Lozeron, P. and Lacroix, C. (2012) Amyloid neuropathies. Curr. Opin. Neurol. 25 (5), 564572.
[5] Dungu, J.N., Anderson, L.J., Whelan, C.J. and Hawkins, P.N. (2012) Cardiac transthyretin amyloidosis. Heart, http://dx.doi.org/10.1136/heartjnl-2012-301924.
[6] Ubhi, K. and Masliah, E. (2012) Alzheimer's disease: recent advances and future perspectives. J. Alzheimers Dis.. 10.3233/JAD-2012-129028.
[7] Masdeu, J.C., Kreisl, W.C. and Berman, K.F. (2012) The neurobiology of Alzheimer disease defined by neuroimaging. Curr. Opin. Neurol. 25 (4), 410–420.
[8] Ferronejames, F.A. and Eaton, W.A. (1985) Kinetics of sickle hemoglobin polymerization II. A double nucleation mechanism. J. Mol. Bio. 183, 611–631.
[9] Morris, A.M., Watzky, M.A. and Finke, R.G. (2009) Protein aggregation kinetics, mechanism, and curve-fitting: a review of the literature. Biophys. Acta 1794 (3), 375–397.
[10] Collins, S.R., Douglass, A., Vale, R.D. and Weissman, J.S. (2004) Mechanism of prion propagation: amyloid growth occurs by monomer addition. PLoS Biol. 10, 1582–1590.
[11] Kellermayer, M.S.Z. et al. (2008) Stepwise dynamics of epitaxially growing single amyloid fibrils. Proc. Natl. Acad. Sci. USA 105, 141.
[12] Fonslet, J. et al. (2010) Stop-and-go kinetics in amyloid fibrillation. Phys. Rev. E (Rapid Commun.) 82, 010901.
[13] Knowles, T.P.J. et al. (2009) An analytical solution to the kinetics of breakable filament assembly. Science 326, 1533.
[14] Cabriolu, R., Kashchiev, D. and Auer, S. (2011) Size distribution of amyloid nanofibrils. Biophys. J. 101, 2232–2241.
[15] Hefendehl, J.K. et al. (2011) Long-term in vivo imaging of β-amyloid plaque appearance and growth in a mouse model of cerebral β-amyloidosis. Neuroscience 31 (2), 624–629.
[16] Ii, K. et al. (1997) Immunocytochemical co-localization of the proteasome in ubiquitinated structures in neurodegenerative diseases and the elderly. J. Neuropathol. Exp. Neurol. 56, 125–131.
[17] Sieradzan, K.A. et al. (1999) Huntington's disease intranuclear inclusions contain truncated, ubiquitinated huntingtin protein. Exp. Neurol. 156 (1), 92–99.
[18] Sawada, H. et al. (2004) Proteasome mediates dopaminergic neuronal degeneration, and its inhibition causes alpha-synuclein inclusions. J. Biol. Chem. 279 (11), 10710–10719.
[19] Rideout, H.J. et al. (2001) Proteasomal inhibition leads to formation of ubiquitin/alpha-synuclein-immunoreactive inclusions in PC12 cells. J. Neurochem. 78 (4), 899–908.
[20] Sun, F. et al. (2006) Proteasome inhibitor MG-132 induces dopaminergic degeneration in cell culture and animal models. Neurotoxicology 27 (5), 807–815.
[21] McNaught, K.S. and Jenner, P. (2001) Proteasomal function is impaired in substantia nigra in Parkinson's disease. Neurosci. Lett. 297 (3), 191–194.
[22] Lindersson, E. et al. (2004) Proteasomal inhibition by alpha-synuclein filaments and oligomers. J. Biol. Chem. 279, 12924–12934.
[23] Petrucelli, L. et al. (2002) Parkin protects against the toxicity associated with mutant alpha-synuclein: proteasome dysfunction selectively affects catecholaminergic neurons. Neuron 36, 1007–1019.
[24] Bence, N.F., Sampat, R.M. and Kopito, R.R. (2001) Impairment of the ubiquitin–proteasome system by protein aggregation. Science 292 (349), 1552–1555.
[25] Emmanouilidou, E., Stefanis L., and Vekrellis, K. (2010) Cell-produced alpha-synuclein oligomers are targeted to, and impair, the 26S proteasome. Neurobiol. Aging. 31 (6), 953–968.

[26] Zhang, N.Y., Tang, Z. and Liu, C.W. (2008) Alpha-Synuclein protofibrils inhibit 26 S proteasome-mediated protein degradation: understanding the cytotoxicity of protein protofibrils in neurodegenerative disease pathogenesis. J. Biol. Chem. 283 (29), 20288–20298.
[27] Narendra, D. et al. (2008) Parkin is recruited selectively to impaired mitochondria and promotes their autophagy. J. Cell. Biol. 183, 795–803.
[28] Cuervo, A.M. et al. (2004) Impaired degradation of mutant alpha-synuclein by chaperone-mediated autophagy. Science 305 (3505), 1292–1295.
[29] Kirkin, V. et al. (2009) A role for ubiquitin in selective autophagy. Mol. Cell. 34 (3), 259–269.
[30] Ishihara, N. and Mizushima, N. (2009) A receptor for eating mitochondria. Dev. Cell. 17 (1), 1–2.
[31] Komatsu, M. et al. (2006) Loss of autophagy in the central nervous system causes neurodegeneration in mice. Nature 441, 880–884.
[32] Hara, T. et al. (2006) Suppression of basal autophagy in neural cells causes neurodegenerative disease in mice. Nature 441, 885–889.
[33] Stefanis, L. et al. (2001) Expression of A53T mutant but not wild-type alpha-synuclein in PC12 cells induces alterations of the ubiquitin-dependent degradation system, loss of dopamine release, and autophagic cell death. J. Neurosci. 21, 9549–9560.
[34] Sneppen, K., Lizana, L., Jensen, M.H., Pigolotti, S. and Otzen, D. (2009) Modeling proteasome dynamics in Parkinson's disease. Phys. Biol. 6, 036005.
[35] Griffin, B.A., Adams, S.R. and Tsien, R.Y. (1998) Specific covalent labeling of recombinant protein molecules inside live cells. Science 281, 269–272.
[36] Zuern, A., Klenk, C., Zabel, U., Reiner, S., Lohse, M.J. and Hoffmann, C. (2010) Site-specific, orthogonal labeling of proteins in intact cells with two small biarsenical fluorophores. Bioconjugate Chem. 21, 853–859.
[37] Berg, I., Nilsson, K.P.R., Thor, S. and Hammarstrom, P. (2010) Efficient imaging of amyloid deposits in Drosophila models of human amyloidoses. Nat. Protoc. 5, 935–944.
[38] Gillespie, D.T. (1977) Exact stochastic simulation of coupled chemical reactions. J. Phys. Chem. 81, 2340.
[39] Knowles, T.P.J. et al. (2007) Kinetics and thermodynamics of amyloid formation from direct measurements of fluctuations in fibril mass. Proc. Natl. Acad. Sci. 104, 24.
[40] Kusumoto, Y., Lomakin, A., Teplow, D.B. and Benedek, G.B. (1998) Temperature dependence of amyloid β-protein fibrillization. Proc. Natl. Acad. Sci. 95, 12277–12282.
[41] Huot, P., Levesque, M. and Parent, A. (2007) The fate of striatal dopaminergic neurons in Parkinson's disease and Huntington's chorea. Brain 130, 222–232.
[42] Tanaka, K. and Ichihara, A. (1989) Half-life of proteasomes (multiprotease complexes) in rat liver. Biochem. Biophys. Res. Commun. 159, 1309–1315.
[43] Cuervo, A.M., Palmer, A., Rivett, A.J. and Knecht, E. (1995) Degradation of proteasomes by lysosomes in rat liver. Eur. J. Biochem. 227, 792–800.